Journal of the Physical Society of Japan
Vol. 71, No. 1, January, 2002, pp. 347–356

Polarization Dependence of Resonant X-Ray Emission Spectra in $3d^n$ Transition Metal Compounds with $n = 0, 1, 2, 3$

Masahiko MATSUBARA, Takayuki UOZUMI[1], Akio KOTANI, Yoshihisa HARADA[2] and Shik SHIN

Institute for Solid State Physics, The University of Tokyo, 5-1-5 Kashiwanoha, Kashiwa-shi, Chiba 277-8581
[1]*College of Engineering, Osaka Prefecture University, Sakai, Osaka 593-8531*
[2]*The Institute of Physical and Chemical Research (RIKEN), Sayo-gun, Hyogo 679-5143*

(Received August 3 2001)

The polarization dependence of $2p \rightarrow 3d \rightarrow 2p$ resonant X-ray emission spectroscopy (RXES) in $3d^1$, $3d^2$ and $3d^3$ systems (TiF_3, VF_3 and Cr_2O_3, respectively) is measured and analyzed by means of the MX_6 (M denotes a transition metal and X denotes a ligand, respectively) cluster model. The results are compared with a previous one for the $3d^0$ system (TiO_2). Generally, with increasing $3d$ electron number, the spectral structure of RXES becomes more complicated by the influence of the crystal field and the multiplet coupling effect. Moreover, we point out that the selection rules on the polarization dependence of RXES change with the $3d$ electron number and that a drastic resonance enhancement corresponding to the excitation to an antibonding state in the $3d^0$ system is almost absent for the $3d^n$ systems with $n = 1$, 2 and 3.

KEYWORDS: resonant X-ray emission, polarization dependence, transition metal compounds, cluster model, multiplet coupling, hybridization effect, Wigner–Eckart theorem
DOI: 10.1143/JPSJ.71.347

1. Introduction

Resonant X-ray emission spectroscopy (RXES) is a useful tool to analyze the electronic structures of transition metal compounds[1–3] due to the recent development of high brightness synchrotron radiation light sources. In RXES a core electron is excited near the threshold by an incident photon, and then the excited state decays by emitting an X-ray photon. Hence, the whole process of RXES is described by a coherent second order optical process.[4,5]

The polarization dependence in RXES is a new interesting topic.[6,7] Recently we studied the $2p \rightarrow 3d \rightarrow 2p$ RXES of TiO_2 and ScF_3 in ''polarized'' and ''depolarized'' configurations, and showed a drastic polarization dependence both theoretically and experimentally.[7,8] We call TiO_2 and ScF_3 ''$3d^0$ system'', because tetravalent Ti and trivalent Sc have nominally no $3d$ electron. The ''polarized'' configuration is the case where the polarization vector of the incident photon is perpendicular to the scattering plane and the ''depolarized'' configuration is the case where it is parallel to the scattering plane. In both configurations, the scattering angle is fixed to 90° and the polarization of the emitted photon is not detected (see Fig. 1).

The calculated results of the Ti $2p$ X-ray absorption spectroscopy (XAS) and $2p \rightarrow 3d \rightarrow 2p$ RXES using a TiO_6 cluster model are shown in Fig. 2(a) and 2(b),[8] respectively. It is seen that an elastic peak at 0 eV and an inelastic peak at 14 eV are allowed for the polarized configuration but forbidden for the depolarized configuration, while weak inelastic structures at 7–9 eV are allowed for both configurations. The intensity of the elastic peak is enhanced for the incident photon energy tuned at the main peaks (**b**, **d**, etc.) of XAS, while that of the 14 eV inelastic peak is dramatically enhanced at weak satellite structures (**g** and **h**) of XAS. These features of RXES in TiO_2 (and similar behavior in ScF_3) were successfully observed experimentally,[7,8] and the mechanism of the resonance behavior and the characteristic polarization dependence of RXES is explained well on the basis of the symmetry of bonding, nonbonding and antibonding states between d^0 and $d^1\underline{L}$ configurations of the $3d^0$ system, where $\underline{L}$ denotes a ligand hole.

It is the purpose of the present paper to measure experimentally and analyze theoretically the polarization-dependent RXES spectra for $3d^1$, $3d^2$ and $3d^3$ systems, and compare the results with the $3d^0$ systems. As typical systems we choose TiF_3 ($3d^1$), VF_3 ($3d^2$) and Cr_2O_3 ($3d^3$). In §2, experimental results are shown. In §3 the model and formulation of theoretical calculations are given, and in §4 the calculated results are shown. Section 5 is devoted to discussions on the selection rules in the polarization dependence of RXES in $3d^n$ systems, and the difference in the RXES features between $3d^0$ and $3d^n$ ($n = 1$, 2 and 3) systems.

2. Experimental Results

The RXES experiments of $3d^n$ systems were performed at the undulator beamline BL-2C[9] at Photon Factory, KEK. Synchrotron radiation was monochromatized using a varied-line spacing plain grating whose average groove density is

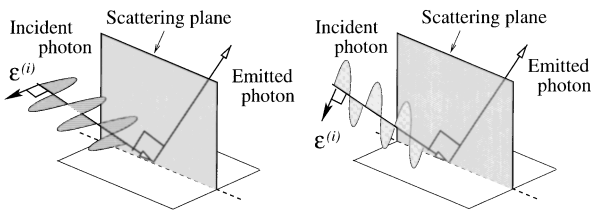

(a) Polarized configuration (b) Depolarized configuration

Fig. 1. Schematic configurations of the experiment. (a) Polarized configuration: the polarization vector of the incident photon ($\varepsilon^{(i)}$) is perpendicular to the scattering plane. (b) Depolarized configuration: the polarization vector of the incident photon is parallel to the scattering plane. In both configurations, scattering angle is fixed to 90°.

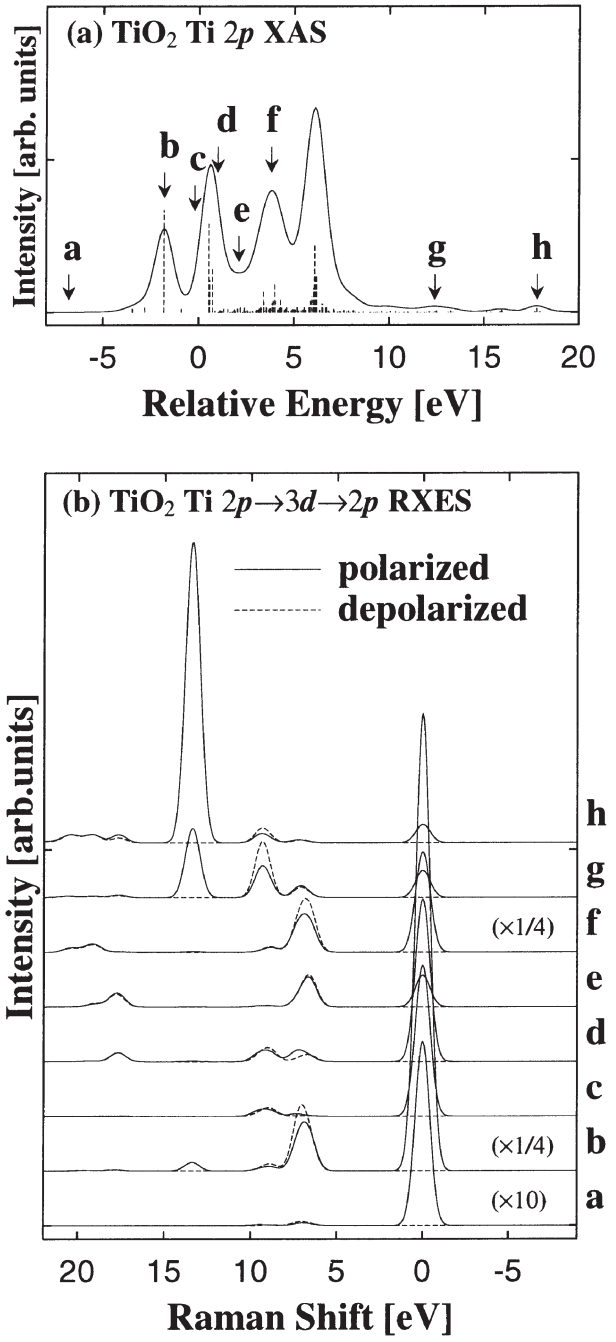

Fig. 2. Calculated results of (a) Ti $2p$ XAS and (b) Ti $2p \rightarrow 3d \rightarrow 2p$ RXES for TiO_2. The RXES spectra in the polarized configuration are plotted by solid lines, while those in the depolarized configuration by dashed lines. Indices from **a** to **h** denote the incident photon energies.

1000 lines/mm. A Rowland mount type soft X-ray emission spectrometer[10] was used for the RXES measurement. It is equipped with a 20 μm width incident slit and a laminar holographic grating whose radius and groove density are 5 m and 1200 lines/mm.

The polarization vector of the incident photon is linear and horizontal, and the emission spectrometer is mounted in a plane normal to the Poynting vector of the incident photon, with 90° rotation along the vector for the polarization dependence. When the spectrometer is in the horizontal and in the vertical position, it corresponds to the "depolarized" and the "polarized" configuration, respectively. The incident angle of the soft X-ray to the sample normal was about 70° to avoid the self-absorption effect. The energy calibration of the incident photon was carried out by the photoemission of gold $4f$ line. The excitation energy resolution of XAS for each sample was about 0.2 eV full width at half maximum (FWHM), whereas the total energy resolutions (including both excitation and emission energy resolutions) of RXES for TiF_3, VF_3 and Cr_2O_3 were about 0.6 eV, 0.7 eV and 0.8 eV (FWHM), respectively. The base pressure of the experimental chamber was kept below 2×10^{-9} Torr.

Pressed pellets of TiF_3, VF_3, and a single crystal of Cr_2O_3 were prepared for the RXES measurements of $3d^n$ systems. The pellets are regarded as polycrystal, and may include many incident photon directions in XAS and RXES measurements. Figures 3(a), 4(a) and 5(a) show XAS spectra of TiF_3, VF_3 and Cr_2O_3 obtained by the total electron yield method (TEY). They are normalized to the incident photon flux. Figures 3(b), 4(b) and 5(b) show the RXES spectra excited at selected energies as denoted by a, b, c, ... in the TEY spectra. The spectra are plotted in the energy-loss from the elastic peaks as the Raman shift energy. The RXES intensities were first normalized to the incident photon flux, and then adjusted to fit the fluorescence structure in the polarized configuration to that in the depolarized configuration. For the vertical bars shown in Figs. 3(b), 4(b) and 5(b), see §4.1.

3. Model and Formulation

We describe these compounds by an MX_6 (M = Ti, V, Cr and X = F, O) cluster model with O_h symmetry. The Hamiltonian is given by

$$H = H_{\rm atom} + H_{\rm CF} + H_{\rm L} + H_{\rm mix}, \tag{3.1}$$

where

$$\begin{aligned} H_{\rm atom} = & \sum_{\nu} \varepsilon_d d_\nu^\dagger d_\nu + \sum_{\mu} \varepsilon_c c_\mu^\dagger c_\mu \\ & + U_{\rm dd} \sum_{\nu>\nu'} d_\nu^\dagger d_\nu d_{\nu'}^\dagger d_{\nu'} - U_{\rm dc} \sum_{\nu,\mu} d_\nu^\dagger d_\nu (1 - c_\mu^\dagger c_\mu) \\ & + H_{\rm multiplet}, \end{aligned} \tag{3.2}$$

$$H_{\rm CF} = \sum_{\nu} \varepsilon(\Gamma) d_\nu^\dagger d_\nu,$$

$$\varepsilon(\Gamma) = \begin{cases} \dfrac{3}{5}(10Dq) & \Gamma = e_g \\ -\dfrac{2}{5}(10Dq) & \Gamma = t_{2g}, \end{cases} \tag{3.3}$$

$$H_{\rm L} = \sum_{\nu} \varepsilon_{\rm L} L_\nu^\dagger L_\nu, \tag{3.4}$$

$$H_{\rm mix} = \sum_{\nu} V(\nu)(d_\nu^\dagger L_\nu + L_\nu^\dagger d_\nu). \tag{3.5}$$

Here $d_\nu^\dagger$ (d_ν), $c_\mu^\dagger$ (c_μ), $L_\nu^\dagger$ (L_ν) are electron creation (annihilation) operators for M $3d$, core, X $2p$ orbitals, respectively. ν and μ denote the combined indices representing the spin (σ) and orbital (Γ) states, and Γ runs over t_{2g} and e_g, which are irreducible representations of O_h. The first term $H_{\rm atom}$ describes the M atomic state including the M $2p$ and $3d$ states. The second term $H_{\rm CF}$ describes the

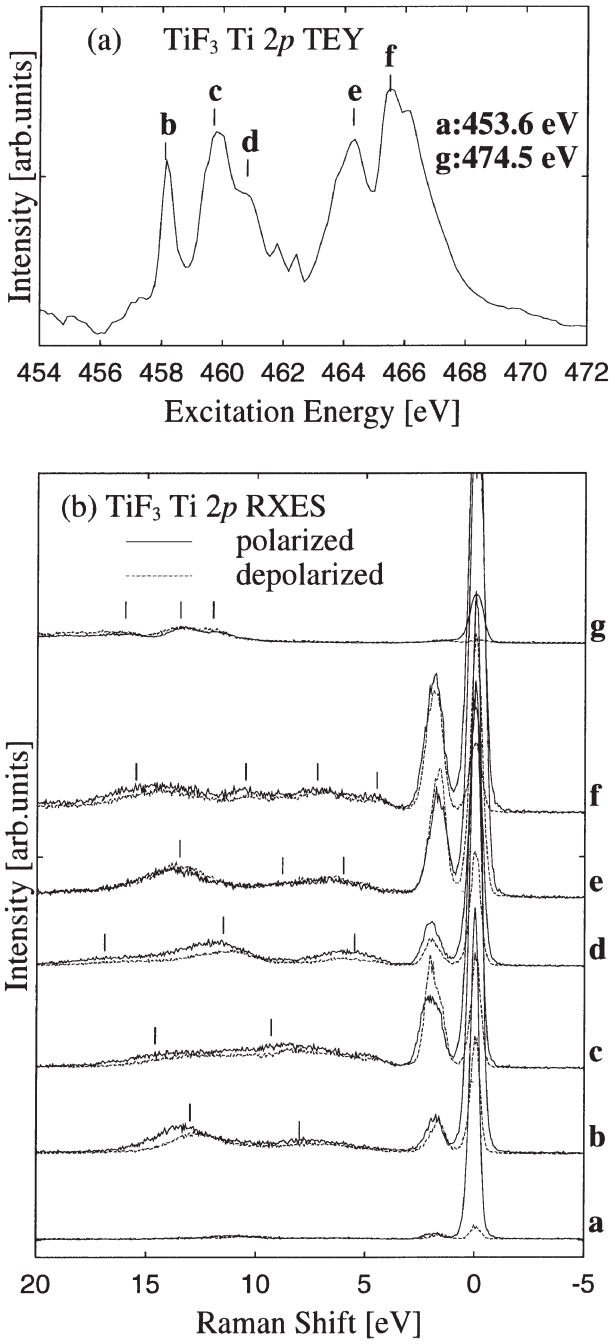

Fig. 3. Experimental results of (a) Ti $2p$ XAS and (b) Ti $2p \rightarrow 3d \rightarrow 2p$ RXES for TiF_3. The RXES spectra in the polarized configuration are plotted by solid lines, while those in the depolarized configuration by dashed lines. Indices from **a** to **g** denote the incident photon energies.

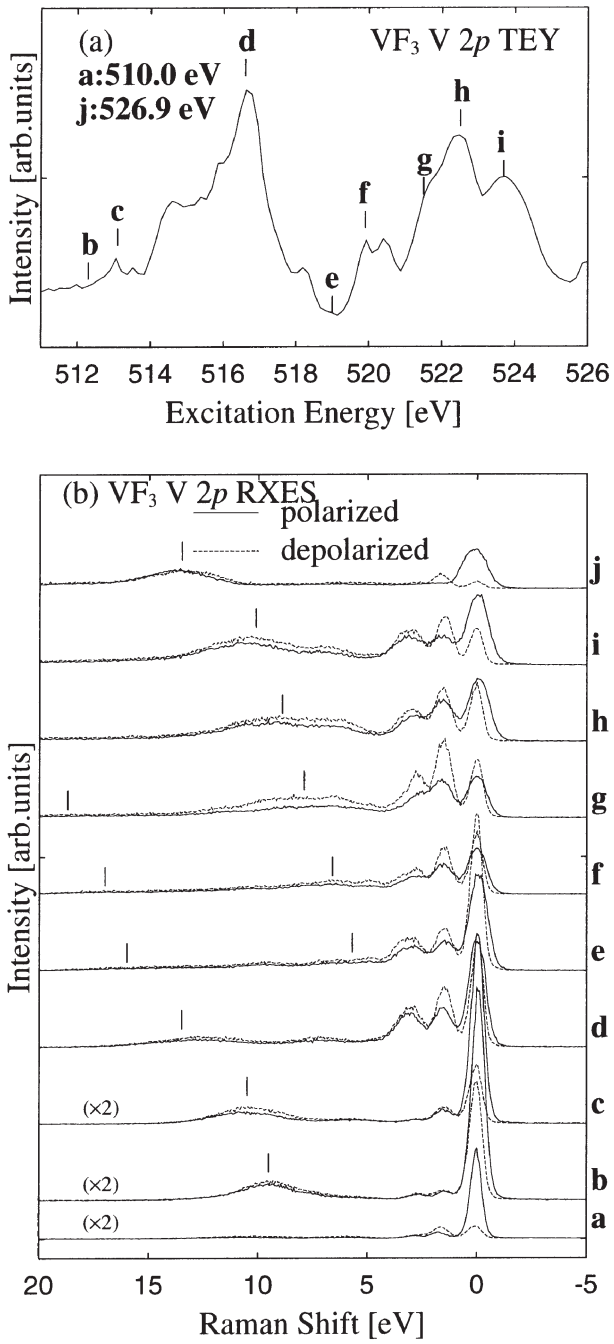

Fig. 4. Experimental results of (a) V $2p$ XAS and (b) V $2p \rightarrow 3d \rightarrow 2p$ RXES for VF_3. The RXES spectra in the polarized configuration are plotted by solid lines, while those in the depolarized configuration by dashed lines. Indices from **a** to **j** denote the incident photon energies.

crystal field splitting. The third and fourth terms, H_{L} and H_{mix}, describe the X $2p$ molecular orbitals and the hybridization between the M $3d$ state and the X $2p$ molecular orbitals.

The first and second terms of H_{atom} denote the one particle energies for the M $3d$ and $2p$ states, respectively, the third and fourth terms denote the Coulomb interaction U_{dd} between $3d$ electrons and the attractive core–hole potential $-U_{\mathrm{dc}}$ acting on the $3d$ electrons, respectively. The last term denotes the intra-atomic multiplet coupling originating from the multipole components of the Coulomb interaction between the M $3d$ states and that between the M $3d$ and $2p$ states. The spin-orbit interactions for the M $3d$ and $2p$ states are also included in $H_{\mathrm{multiplet}}$.

The charge transfer (CT) energy Δ is defined as $\Delta = E(d^{n+1}\underline{L}) - E(d^n)$ with $n = 1$, 2 and 3 for TiF_3, VF_3 and Cr_2O_3, where $\underline{L}$ denotes a hole in the X $2p$ orbital and $E(d^1\underline{L})$ and $E(d^0)$ denote the multiplet averaged energies of the $d^{n+1}\underline{L}$ and d^n configurations, respectively. In these calculations, we treat Δ, U_{dd}, U_{dc}, $V(e_g)$ $[= -2V(t_{2g})$, for simplicity], and the crystal field splitting energy $10Dq$ $[= \varepsilon(e_g) - \varepsilon(t_{2g})]$ as adjustable parameters. The Slater integrals F^k and G^k, and the spin-orbit coupling constant ζ are obtained by the atomic Hartree–Fock calculation, and then the Slater integrals are reduced to 85%.

The initial state of RXES, $|g\rangle$ is denoted by a linear

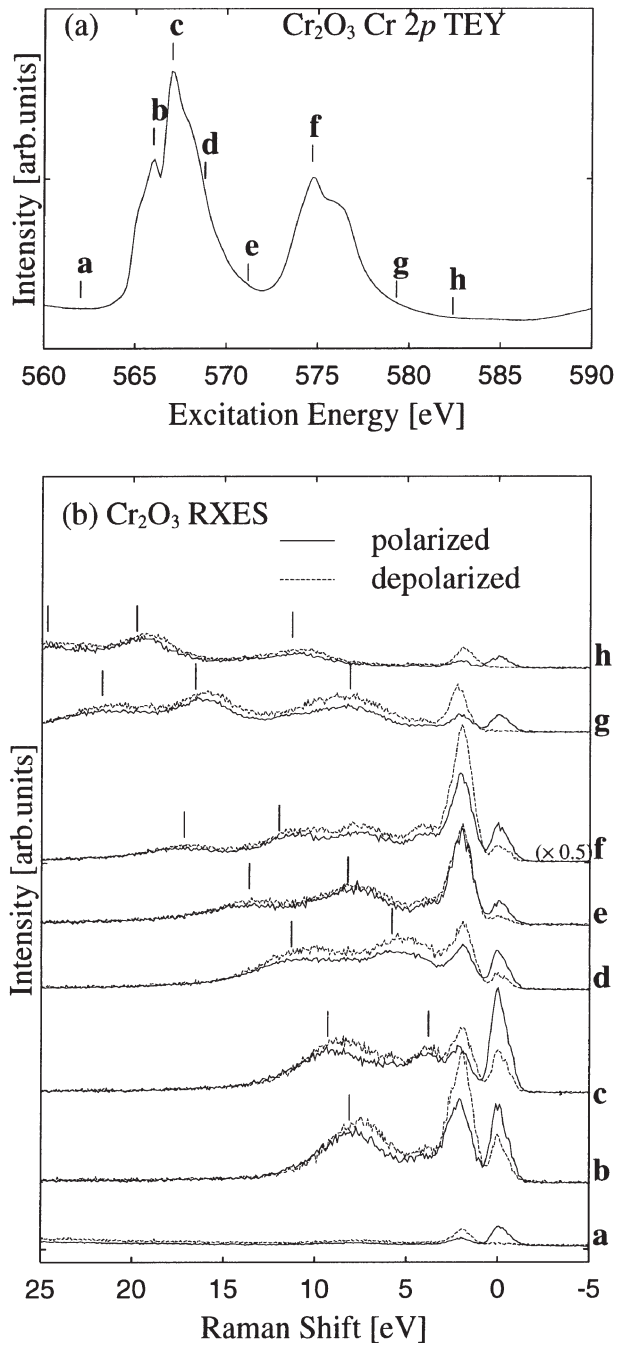

Fig. 5. Experimental results of (a) Cr $2p$ XAS and (b) Cr $2p \rightarrow 3d \rightarrow 2p$ RXES for Cr_2O_3. The RXES spectra in the polarized configuration are plotted by solid lines, while those in the depolarized configuration by dashed lines. Indices from **a** to **h** denote the incident photon energies.

combination of three configurations:

$$|g\rangle = c_0|d^n\rangle + c_1|d^{n+1}\underline{L}\rangle + c_2|d^{n+2}\underline{L}^2\rangle. \tag{3.6}$$

TiF_3, VF_3 and Cr_2O_3 correspond to the case of $n = 1$, 2 and 3, respectively. These three configurations are mixed with one another through the hybridization. The final state is also given by the same form as eq. (3.6). On the other hand, since a M $2p$ core electron is excited to an empty M $3d$ orbital in the intermediate state of RXES (the final state of $2p$–XAS), the intermediate state is written as follows:

$$|m\rangle = c_0'|\underline{c}d^{n+1}\rangle + c_1'|\underline{c}d^{n+2}\underline{L}\rangle + c_2'|\underline{c}d^{n+3}\underline{L}^2\rangle. \tag{3.7}$$

Here, $\underline{c}$ denotes a hole in the core ($2p$) level. The Hamiltonian (3.1) is diagonalized by these bases. The XAS spectrum is expressed as

$$F_{\mathrm{XAS}}(\Omega) = \sum_m |\langle m|T_1|g\rangle|^2 \delta(\Omega - E_m + E_g), \tag{3.8}$$

where Ω denotes the incident photon energy, $|g\rangle$ and $|m\rangle$ are the ground and final states of XAS with energies E_g and E_m, respectively. The RXES spectrum is expressed as

$$F(\Omega,\omega) = \sum_f \left| \sum_m \frac{\langle f|T_2|m\rangle\langle m|T_1|g\rangle}{E_m - E_g - \Omega - \mathrm{i}\Gamma_m} \right|^2 \times \delta(\Omega - \omega + E_g - E_f), \tag{3.9}$$

where $|g\rangle$, $|m\rangle$ and $|f\rangle$ represent the ground, intermediate and final states of RXES with energies E_g, E_m and E_f, respectively. T_1 and T_2 are the electric dipole transition operators. The incident and emitted photon energies are represented by Ω and ω, respectively. The Raman shift energy is defined as the difference between the incident and emitted photon energies, i.e. $\Omega - \omega$.

In the calculation of RXES spectra, the direction of the incident photon propagation is taken parallel to the cubic axis (i.e. in the M–X direction of the MX_6 cluster) for simplicity. This is a good approximation, because the RXES spectra are unchanged (or almost unchanged, depending on the symmetry of the final state) with the change of the incident photon direction in our calculations, where the symmetry of the system is O_h and the scattering angle is 90°. Then, eq. (3.9) is transformed, for the polarized and depolarized configurations, into the following forms:[8)]

$$F(\Omega,\omega) = \sum_f \left| \sum_{q,q'=\pm1} \sum_m \frac{\langle f|C_q^{(1)}|m\rangle\langle m|C_{q'}^{(1)}|g\rangle}{E_m - E_g - \Omega - \mathrm{i}\Gamma_m} \right|^2 \times \delta(\Omega - \omega + E_g - E_f) \quad \text{(polarized)}, \tag{3.10}$$

$$F(\Omega,\omega) = \sum_f \left| \sum_{q=\pm1} \sum_m \frac{\langle f|C_q^{(1)}|m\rangle\langle m|C_0^{(1)}|g\rangle}{E_m - E_g - \Omega - \mathrm{i}\Gamma_m} \right|^2 \times \delta(\Omega - \omega + E_g - E_f) \quad \text{(depolarized)}. \tag{3.11}$$

4. Calculated Results

In this section we show the calculated results of XAS and polarization dependent RXES of TiF_3, VF_3 and Cr_2O_3. The parameter values used in this calculation are shown in Table I. For comparison, those for TiO_2 are also listed in the table. The parameter values of TiF_3 and VF_3 are based on those of ScF_3[11)] and adjusted so as to reproduce experimental results, whereas those of Cr_2O_3 are almost the same as those given by Uozumi *et al.*[12)] and Taguchi[13)] but

Table I. Adjustable parameter values in eV in the model Hamiltonian eq. (3.1), and the parameters R_c, R_v for the configuration dependence of hybridization strength.

Compounds	Δ	U_{dd}	U_{dc}	$V(e_g)$	$10Dq$	R_c	R_v
TiO_2	2.98	4.0	6.0	3.4	1.7	0.8	0.9
TiF_3	8.5	6.4	8.0	3.0	1.5	0.8	0.9
VF_3	8.0	6.0	7.5	2.9	1.4	0.8	0.9
Cr_2O_3	5.5	5.5	6.5	3.0	1.3	0.8	0.9

slightly changed in order to consider the configuration dependence of hybridization strength.[14)]

In order to take into account the configuration dependence of hybridization strength we introduce two factors R_c and R_v:[15)] Since the M $3d$ wave function is contracted when a $2p$ hole is created, the hybridization strength $V(\Gamma)$ between $3d^0$ and $3d^1\underline{L}$ configurations is reduced to $R_c V(\Gamma)$ between $\underline{c}3d^0$ and $\underline{c}3d^1\underline{L}$ configurations. Meanwhile, the hybridization between $3d^1\underline{L}$ and $3d^2\underline{L}^2$ is enhanced to $V(\Gamma)/R_v$ because the $3d$ wave function is more extended with increasing $3d$ electron number (R_c and R_v being both less than unity).

XAS spectra are convoluted with the Lorentzian and Gaussian functions with the half width at half maximum (HWHM) of $\Gamma_L = 0.1$ eV (for TiF_3) and 0.2 eV (for VF_3 and Cr_2O_3), and $\Gamma_G = 0.5$ eV, respectively, while RXES spectra with only the Gaussian functions with the same HWHM value (0.5 eV) as XAS.

4.1 TiF_3

In Fig. 6(a), we show the calculated result of Ti $2p$–XAS for TiF_3. On the low energy side of Ti $2p$–XAS, the result is not in good agreement with the experimental one [Fig. 3(a)]. In particular, we can see very intense peak at **b** in the experiment, but in the calculation, although the structure is seen, we cannot see such an intense peak. The reason for the difference is not clear at present.

In Fig. 6(b), the calculated result of Ti $2p \rightarrow 3d \rightarrow 2p$ RXES for TiF_3, in which the spectra obtained for the polarized configuration (solid line) and the depolarized configuration (dashed line), are plotted as a function of Raman shift energy. Indices from **a** to **g** indicate incident photon energies and correspond to those in XAS [Fig. 6(a)]. An inelastic peak, which is not seen in the $3d^0$ system is seen at about 2 eV, in agreement with the experimental result [Fig. 3(b)]. This structure originates from the crystal field excitation from T_{2g} to E_g state, i.e. so-called d–d excitation. When the incident photon energies are set to the range from **b** to **f** where the XAS spectrum has large intensity, the elastic peaks have considerably large intensities in both the polarized and depolarized configurations. This is in contrast with the case of the $3d^0$ system, where the elastic peaks are enhanced only in the polarized configuration. This behavior of the elastic peak intensity is in fair agreement with the experimental result.

There are weak structures between about 10 eV and 14 eV in addition to the structures mentioned above, but there occurs no strong resonance corresponding to the 14 eV inelastic peak (i.e. excitation to the antibonding state) in TiO_2.

The structures between 10 eV and 14 eV are not in good agreement with experimental results. The main experimental structures with Raman shifts above 5 eV are shown with vertical bars in Fig. 3(b). These vertical bars represent a series of spectra whose emitted photon energy is almost constant, and in this sense these spectra are similar to those of the normal X-ray emission spectroscopy (NXES), which usually occur for the incident photon energy well above the XAS threshold. These NXES-like spectra near the XAS threshold cannot be reproduced theoretically with our cluster model including a single M atom. Idé and Kotani[16)] studied the origin of the NXES-like spectra, and attributed it to the effect of multi M atoms (i.e., effect of large cluster). The NXES-like spectra (vertical bars) are also observed in VF_3 [Fig. 4(b)] and Cr_2O_3 [Fig. 5(b)], but we will not compare them with our calculated results, because their occurrence is beyond the scope of the present paper.

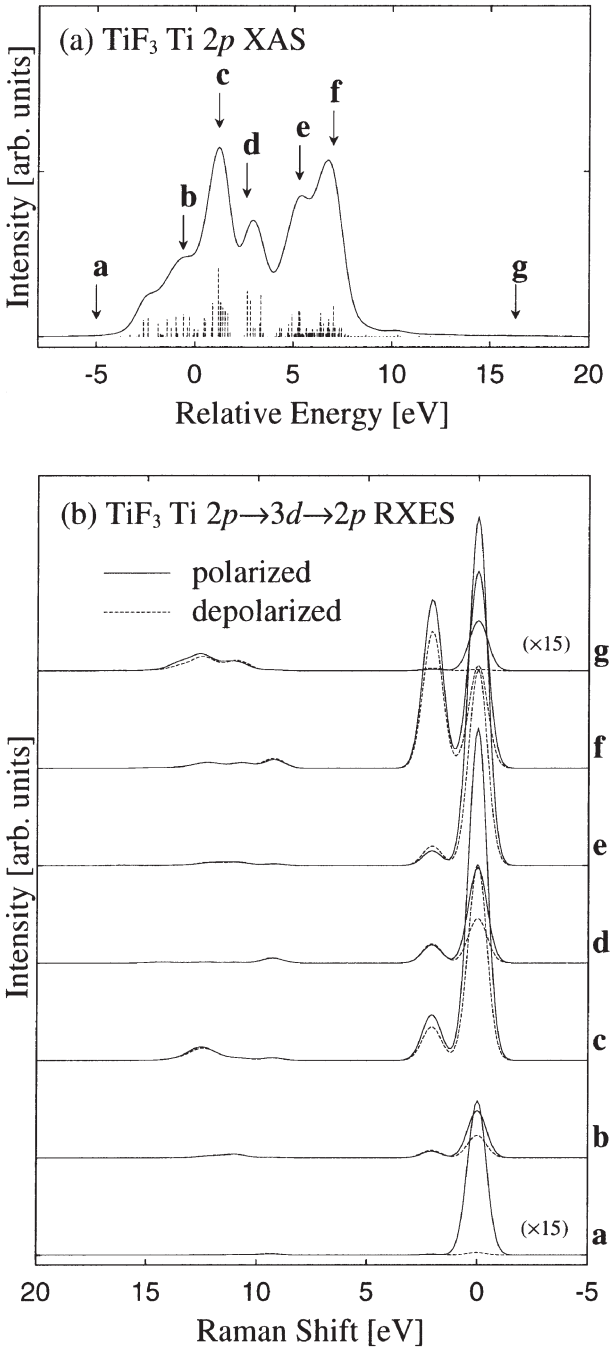

Fig. 6. Calculated results of (a) Ti $2p$ XAS and (b) Ti $2p \rightarrow 3d \rightarrow 2p$ RXES for TiF_3. The RXES spectra in the polarized configuration are plotted by solid lines, while those in the depolarized configuration by dashed lines. Indices from **a** to **g** denote the incident photon energies.

4.2 VF_3

The calculated result of V $2p$–XAS for VF_3 is shown in Fig. 7(a). This is generally in accordance with the experimental one. Structure **d** and its lower energy shoulder, and structures **h** and **i** correspond to four main peaks originating from the spin–orbit splitting and the crystal field

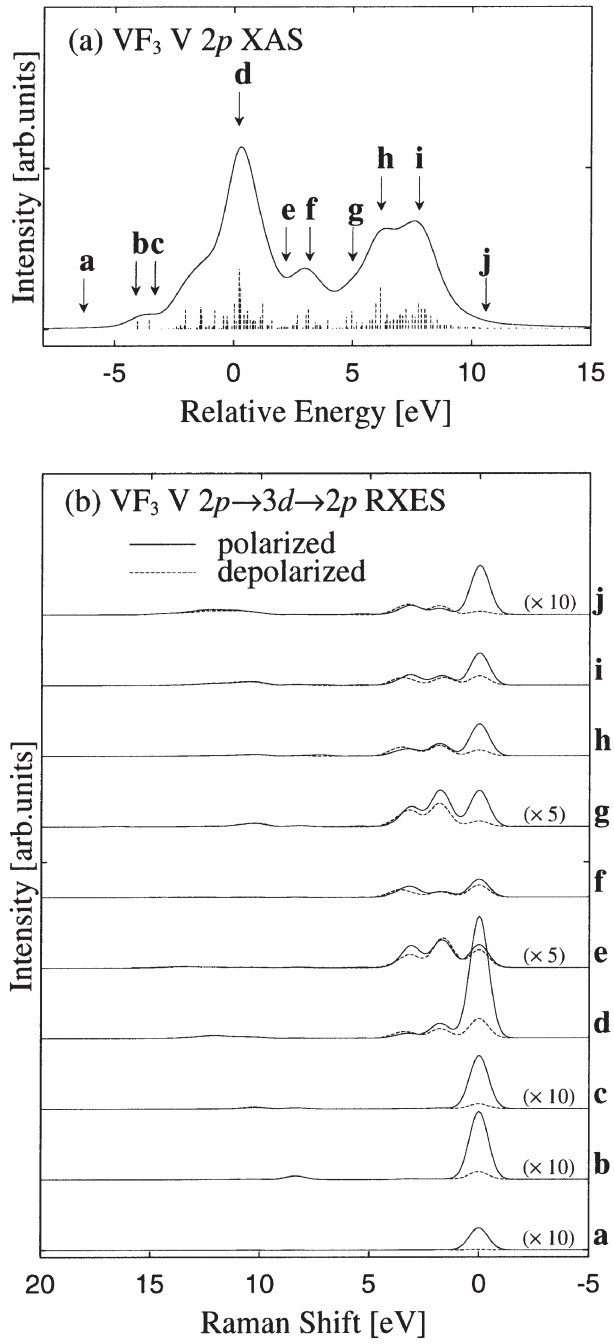

Fig. 7. Calculated results of (a) V $2p$ XAS and (b) V $2p \rightarrow 3d \rightarrow 2p$ RXES for VF_3. The RXES spectra in the polarized configuration are plotted by solid lines, while those in the depolarized configuration by dashed lines. Indices from **a** to **j** denote the incident photon energies.

splitting.

In Fig. 7(b), we show the calculated result of V $2p \rightarrow 3d \rightarrow 2p$ RXES for VF_3, and the spectra obtained for the polarized configuration (solid line) and the depolarized configuration (dashed line) are plotted as a function of Raman shift energy. Indices from **a** to **j** indicate incident photon energies corresponding to those in XAS [Fig. 7(a)]. We can also see structures arising from d–d excitation but they are more complicated than those of TiF_3 due to the effect of multiplet coupling between $3d$ electrons, in addition to the crystal field excitation. When the incident photon energies are set to positions **d**, **g**, **h** and **i**, where XAS structures are considerably strong, the elastic peaks are also enhanced both in the polarized and depolarized configurations. There are weak structures between about 8 eV and 12 eV, in addition to the structures mentioned above. There is no strong resonance corresponding to excitation to the antibonding state.

4.3 Cr_2O_3

In Fig. 8(a), the calculated result of Cr $2p$–XAS for Cr_2O_3 is given and this is in good agreement with the experimental one. In Fig. 8(b), the calculated result of Cr $2p \rightarrow 3d \rightarrow 2p$ RXES for Cr_2O_3 is given and spectra obtained both in the polarized and depolarized configurations (solid and dashed line, respectively) are plotted as a function of Raman shift.

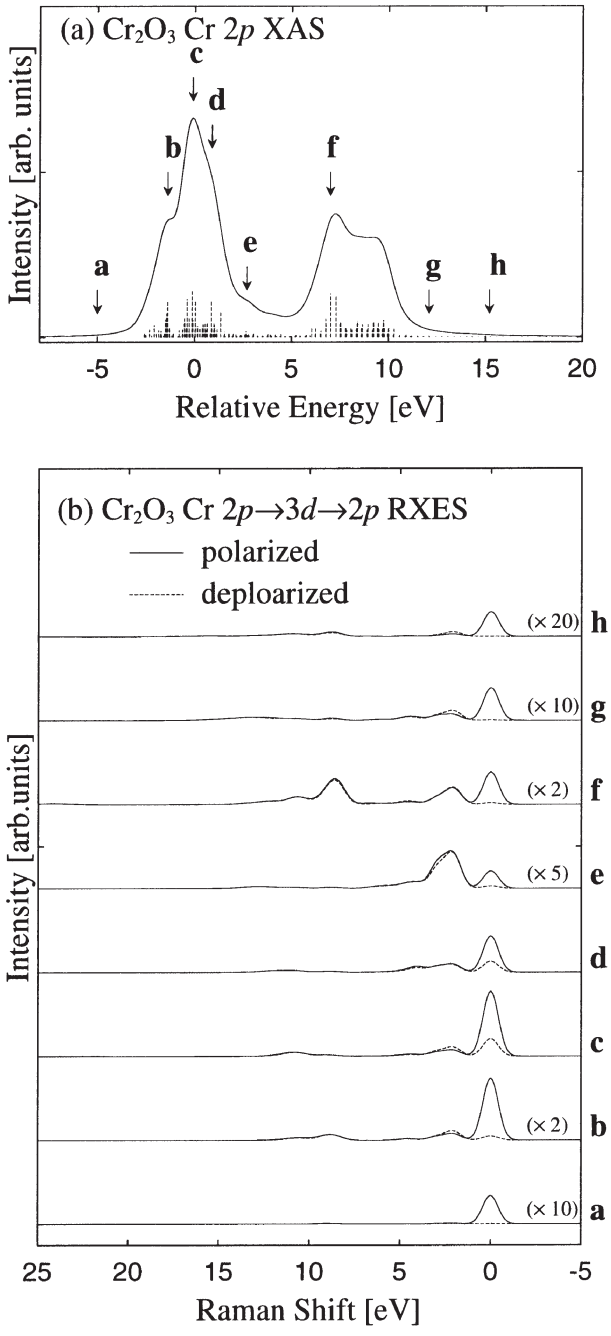

Fig. 8. Calculated results of (a) Cr $2p$ XAS and (b) Cr $2p \rightarrow 3d \rightarrow 2p$ RXES for Cr_2O_3. The RXES spectra in the polarized configuration are plotted by solid lines, while those in the depolarized configuration by dashed lines. Indices from **a** to **h** denote the incident photon energies.

Indices from **a** to **h** denote the incident photon energies corresponding to those in XAS [Fig. 8(a)]. We can see structures at about 2 eV arising from *d*–*d* excitation. In the depolarized configuration, the elastic peaks are absent or very weak. There is no strong resonance corresponding to the antibonding state excitation. These features are in good agreement with the experimental ones [Fig. 5(b)].

5. Discussion

We first discuss the effects of charge transfer in RXES of $3d^n$ compounds. In Fig. 9, we show the total energy level scheme of the $3d^n$ compounds ($n = 0$, 1, 2 and 3), where only the two lowest energy configurations are included and the spin-orbit splitting of the $2p$ states and the crystal field splitting of the $3d$ states are neglected for simplicity.

We can realize that the initial and final states consist of bonding and antibonding states which is formed by strongly hybridized $3d^n$ and $3d^{n+1}\underline{L}$ configurations, and nonbonding states with the $3d^{n+1}\underline{L}$ configuration. On the other hand, the intermediate state consists of bonding and antibonding states formed by strongly hybridized $\underline{c}3d^{n+1}$ and $\underline{c}3d^{n+2}\underline{L}$ configurations, and nonbonding $\underline{c}3d^{n+2}\underline{L}$ states. Therefore, the elastic and inelastic peaks in RXES correspond, respectively, to the bonding final state and the nonbonding and antibonding final states. This situation is common to all of TiO_2, TiF_3, VF_3 and Cr_2O_3, but the behavior of RXES is different in each material. We have already shown in the last section that the crystal field excitation is absent in TiO_2, clearly seen as a single peak in TiF_3, and modified by multiplet coupling effect in VF_3 and Cr_2O_3, due to the difference in the $3d$ electron number.

In the following, we discuss the reason for the difference in the polarization dependence and the antibonding resonance behavior in these materials, on the basis of the difference of the symmetry in the electronic states and the difference in the hybridization and multiplet coupling strengths. In Table II, we show the symmetry of the ground state, the charge transfer energy Δ, the effective hybridization strength of the initial (and also final) state $V_{\rm eff}$, the ratio of Δ to $V_{\rm eff}$ and the average $3d$ electron number in the ground state. $V_{\rm eff}$ is the effective hybridization in which we take into account the effect of empty $3d$ states. $V_{\rm eff}$ for the $3d^n$ systems ($n \leq 6$) is given by

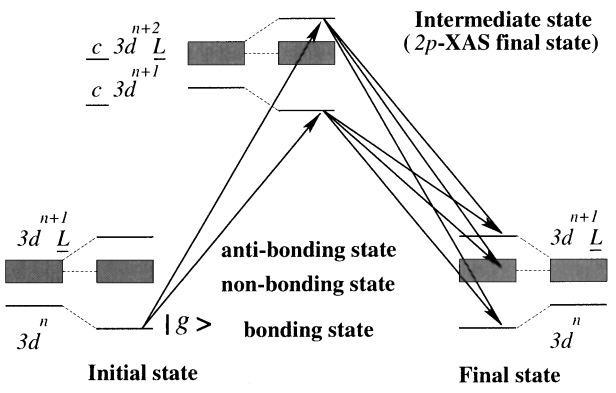

Fig. 9. Total energy level scheme for $2p \rightarrow 3d \rightarrow 2p$ RXES of $3d^n$ compounds ($n = 0$, 1, 2 and 3).

Table II. Symmetry of the ground state, the charge transfer energy Δ and the effective hybridization $V_{\rm eff}$ for TiF_3, VF_3 and Cr_2O_3. $n_{\rm d}$ is the average electron number of the ground state. The values for TiO_2 are also given.

Compounds	Symmetry	Δ (eV)	$V_{\rm eff}$ (eV)	$V_{\rm eff}/\Delta$	$n_{\rm d}$
TiO_2	A_{1g}	2.98	7.97	2.68	0.84
TiF_3	T_{2g}	8.5	6.87	0.81	1.34
VF_3	T_{1g}	8.0	6.48	0.81	2.37
Cr_2O_3	A_{2g}	5.5	6.54	1.19	3.50

$$V_{\rm eff} = \sqrt{(6-n)V(t_{2g})^2 + 4V(e_g)^2}, \tag{5.1}$$

when $n = 0$, 1, 2 and 3 for TiO_2, TiF_3, VF_3 and Cr_2O_3, respectively.

Let us discuss the polarization dependence of RXES spectra by group theoretical consideration. Here we neglect spin–orbit interaction for simplicity although it is included in the calculation in §4. The ground state symmetry (Γ_g) of the $3d^0$, $3d^1$, $3d^2$ and $3d^3$ systems are A_{1g}, T_{2g}, T_{1g} and A_{2g}, respectively. According to the Wigner–Eckart theorem,[17] an optical transition matrix element is described as the Clebsch-Gordan (CG) coefficient:

$$\langle \alpha\Gamma\gamma|T_{\overline{\gamma}}(\overline{\Gamma})|\alpha'\Gamma'\gamma'\rangle \propto \langle \Gamma\gamma|\Gamma'\gamma'\overline{\Gamma}\overline{\gamma}\rangle. \tag{5.2}$$

Here, $\Gamma(\Gamma', \overline{\Gamma})$ denotes an irreducible representation of the group, $\gamma(\gamma', \overline{\gamma})$ the basis of the irreducible representation and $\alpha(\alpha')$ a quantum number other than $\Gamma, \gamma(\Gamma', \gamma')$. Since only the electric dipole transition is considered here, $\overline{\Gamma}$ is T_{1u}. A transition occurs only when the CG coefficient is non-zero. In the polarized and depolarized configurations, we take the polarization of the incident photon in the y and z directions, respectively, where the y direction is normal to the scattering plane (zx plane), so the possible basis of T_{1u} is y and z, respectively. The transition from the ground state to the intermediate states is allowed only when $\langle \Gamma\gamma|T_y(T_{1u})|\Gamma_g\gamma'\rangle$ (polarized configuration) and $\langle \Gamma\gamma|T_z(T_{1u})|\Gamma_g\gamma'\rangle$ (depolarized configuration) are non-zero. In the transition from the intermediate to final states, which is also the dipole transition, the polarization of the emitted photon is both in the x and y directions, i.e. the possible basis of T_{1u} is x and y. Analogous to the absorption process, the emission process (transition from the intermediate to final states) is allowed only when the matrix elements are non-zero. After all, the irreducible representations allowed in the final state of the $3d^0$, $3d^1$, $3d^2$ and $3d^3$ systems, respectively, are given by eqs. (5.3), (5.4), (5.5) and (5.6):

$$\begin{cases} \displaystyle\sum_{\gamma'=x,y} A_{1g} \otimes T_{1u,y} \otimes T_{1u,\gamma'} = A_{1g}, E_g, T_{1g}, T_{2g} \\ \qquad\qquad\qquad\qquad\qquad\qquad \text{(polarized)} \\ \displaystyle\sum_{\gamma'=x,y} A_{1g} \otimes T_{1u,z} \otimes T_{1u,\gamma'} = T_{1g}, T_{2g} \\ \qquad\qquad\qquad\qquad\qquad\qquad \text{(depolarized)}, \end{cases} \tag{5.3}$$

$$\begin{cases} \sum_{\gamma'=x,y} T_{2g} \otimes T_{1u,y} \otimes T_{1u,\gamma'} = A_{1g}, A_{2g}, E_g, T_{1g}, T_{2g} \\ \qquad\qquad \text{(polarized)} \\ \sum_{\gamma'=x,y} T_{2g} \otimes T_{1u,z} \otimes T_{1u,\gamma'} = A_{1g}, A_{2g}, E_g, T_{1g}, T_{2g} \\ \qquad\qquad \text{(depolarized)}, \end{cases} \tag{5.4}$$

$$\begin{cases} \sum_{\gamma'=x,y} T_{1g} \otimes T_{1u,z} \otimes T_{1u,\gamma'} = A_{1g}, E_g, T_{1g}, T_{2g} \\ \qquad\qquad \text{(polarized)} \\ \sum_{\gamma'=x,y} T_{1g} \otimes T_{1u,z} \otimes T_{1u,\gamma'} = A_{1g}, A_{2g}, E_g, T_{1g}, T_{2g} \\ \qquad\qquad \text{(depolarized)}, \end{cases} \tag{5.5}$$

$$\begin{cases} \sum_{\gamma'=x,y} A_{2g} \otimes T_{1u,z} \otimes T_{1u,\gamma'} = A_{2g}, E_g, T_{1g}, T_{2g} \\ \qquad\qquad \text{(polarized)} \\ \sum_{\gamma'=x,y} A_{2g} \otimes T_{1u,z} \otimes T_{1u,\gamma'} = T_{1g}, T_{2g} \\ \qquad\qquad \text{(depolarized)}. \end{cases} \tag{5.6}$$

This result is summarized in Table III.

Keeping these selection rules in mind, we first pay attention to the elastic peak, the final state of which is the same as the ground state. In the $3d^0$ and $3d^3$ systems, we see that the transition to the ground state is allowed only in the polarized configuration, and forbidden in the depolarized one. On the other hand, in the $3d^1$ and $3d^2$ systems, transitions are allowed both in the polarized and depolarized configurations. This is consistent with the results of numerical calculations as well as with the experimental results. For TiO_2 ($3d^0$), the elastic peak is allowed only for the polarized configuration. In the case of TiF_3 ($3d^1$) and VF_3 ($3d^2$), the elastic peak is enhanced both in the polarized and depolarized configurations. For Cr_2O_3 ($3d^3$), the elastic peak intensity in the polarized configuration is much larger than that in the depolarized configuration, but a weak elastic peak is observed even in the depolarized configuration. This apparent breaking of the selection rules in the depolarized configuration of Cr_2O_3 is caused by the spin–orbit interaction, by which the dipole allowed excited states can mix with the ground state and the transition becomes weakly allowed. The calculated result neglecting spin–orbit interaction shows the disappearance of elastic peak in the depolarized configuration. Thus the polarization dependence of the elastic peak intensity in these four compounds are fully understood within the selection rules arising from the symmetry of the system. It should also be mentioned that the nonbonding final states (with T_{1g} and T_{2g} symmetries, for instance) are always allowed for both polarized and depolarized configurations and for all the $3d^0$ to $3d^3$ systems.

The symmetry of the antibonding final state is the same as the bonding final state, so that the selection rule for that is the same as the elastic peak. However, the resonance enhancement of the inelastic peak corresponding to the antibonding final state occurs strongly in TiO_2[7,8] when the incident photon energy is tuned to the XAS satellite, but it cannot be seen in the other three compounds. This difference in the behavior of the antibonding state resonance for TiO_2 and the other three compounds can be explained by the difference in the hybridization strength and the multiplet coupling strength.

It is to be noted that in order to observe the structure due to the antibonding state in RXES the hybridization effect is essential both in the intermediate and final states. If the hybridization is weak, the intensity of the antibonding state should be small both in XAS and RXES. One of the measures of the hybridization effect is given by the ratio of the effective hybridization to the charge transfer energy $V_{\rm eff}/\Delta$. From Table II, it is found that the value of $V_{\rm eff}/\Delta$ is 2.68 for TiO_2 ($3d^0$), whereas it is 0.81, 0.81, 1.19 (much smaller than TiO_2) for TiF_3, VF_3 and Cr_2O_3, respectively. In order to see the effect of hybridization explicitly, we have made the calculations of XAS and RXES for Cr_2O_3 by changing artificially the value of $V_{\rm eff}/\Delta$ so as to make it the same as that of TiO_2. The result is shown in Fig. 10(a) and 10(b), where we can see the resonance enhancement due to the antibonding state excitation (at about 14 eV Raman shift) for RXES of **e**, **f**, **g** and **h**, which was almost absent in Fig. 8(b). However, the resonance enhancement factor is much smaller than that of TiO_2.

We would like to point out that the enhancement factor of the antibonding resonance in Cr_2O_3 (and also in TiF_3 and VF_3) are reduced by the effect of multiplet coupling, compared with that in TiO_2. Since the satellite of XAS is the intermediate state of the antibonding resonance of RXES, the stronger the XAS satellite intensity is, the stronger the RXES resonance is induced. In the $2p$–XAS process, the $3d$ electron number in the intermediate state increases by one. This means that if the $3d$ electron number of the ground state is more than one, two or more $3d$ electrons exist in the intermediate state (final state of the XAS) the whole structure of the XAS spectrum are broadened by the multiplet coupling between the $3d$ electrons as well as between the $2p$ and $3d$ electrons. We can see this situation by comparing the line spectra of $2p$–XAS for TiO_2 [Fig. 2(a)] with those for TiF_3, VF_3 and Cr_2O_3 [Figs. 6(a), 7(a) and 8(a), respectively]. Because of this broadening effect, the satellite structures in XAS cannot be seen in the $3d^1$, $3d^2$

Table III. Ground state symmetry and the allowed final state symmetries for each compound.

Compounds	Ground state (Γ_g)	Final states (polarized) (Γ_f)	Final states (depolarized) (Γ_f)
TiO_2 ($3d^0$)	A_1	A_1, E, T_1, T_2	T_1, T_2
TiF_3 ($3d^1$)	T_2	A_1, A_2, E, T_1, T_2	A_1, A_2, E, T_1, T_2
VF_3 ($3d^2$)	T_1	A_1, A_2, E, T_1, T_2	A_1, E, T_1, T_2
Cr_2O_3 ($3d^3$)	A_2	A_2, E, T_1, T_2	T_1, T_2

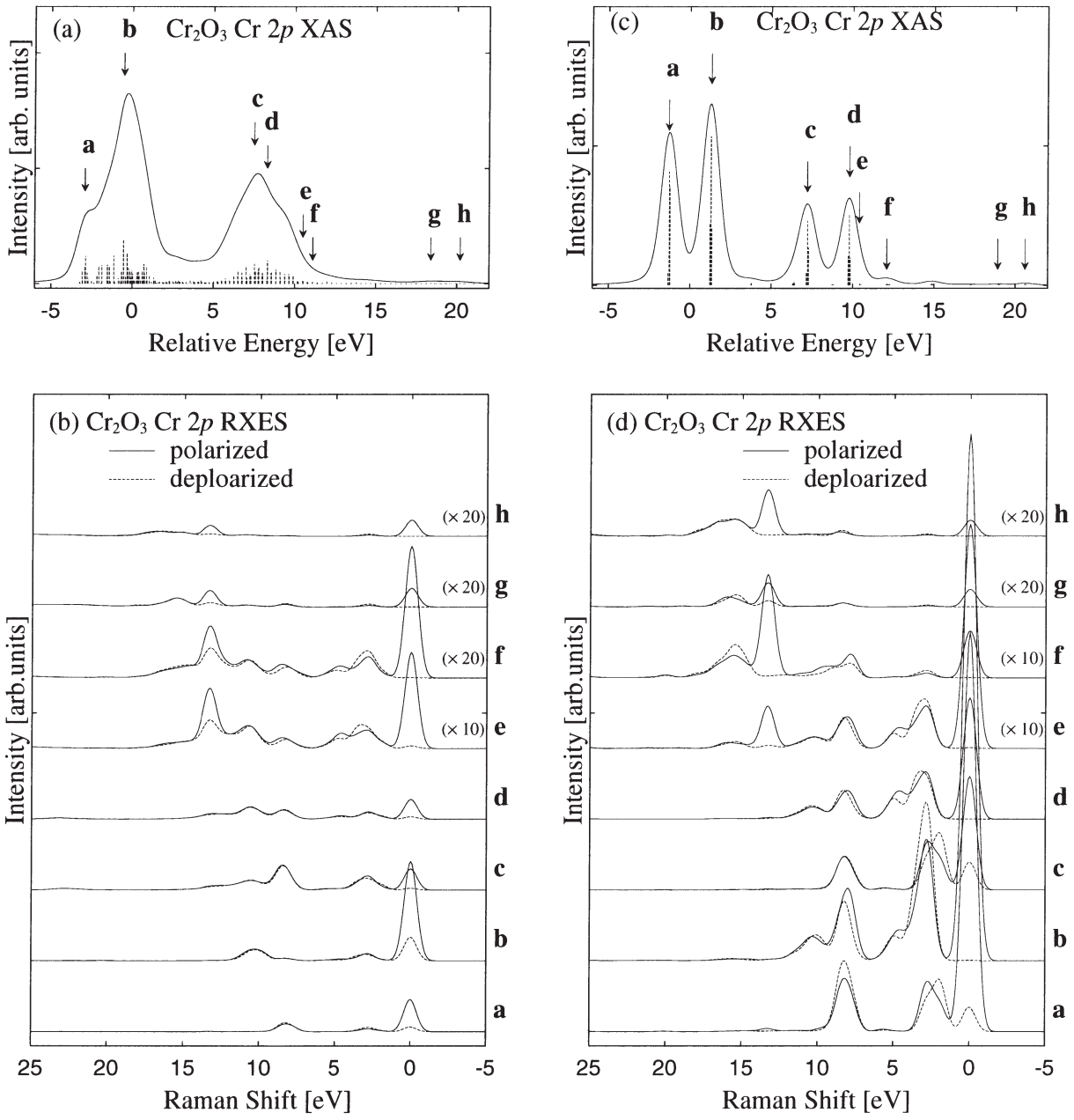

Fig. 10. Calculated results of (a), (c) Cr 2*p* XAS and (b), (d) Cr $2p \rightarrow 3d \rightarrow 2p$ RXES for Cr_2O_3. In (a) and (b) the value of the hybridization effect is the same as that of TiO_2, i.e. $\Delta = 2.98$ eV, $V_{\mathrm{eff}} = 7.97$ eV and $V_{\mathrm{eff}}/\Delta = 2.68$. In (c) and (d) multiplet effect of the intermediate state is neglected.

and $3d^3$ systems, while they are weakly observed in the $3d^0$ system.

In order to see this effect explicitly, we have calculated the XAS and RXES spectra for Cr_2O_3 using the same parameter values as those in the calculation of Fig. 10(a) and 10(b), but neglecting the multiplet coupling in the intermediate state. The result is shown in Fig. 10(c) and 10(d), where the broadening in the XAS spectrum is suppressed and we recognize a stronger antibonding resonance in RXES of **e**, **f**, **g** and **h**.

From the above consideration, the main reason that resonance enhancement of the antibonding peak, which is very strong in the RXES spectra of TiO_2 ($3d^0$ system), is almost absent in the $3d^n$ ($n = 1$, 2 and 3) systems is that (i) the smaller hybridization effect, and (ii) the spectral broadening of XAS due to the multiplet coupling effect.

6. Summary

We measured $2p \rightarrow 3d \rightarrow 2p$ RXES in $3d^1$, $3d^2$ and $3d^3$ systems (TiF_3, VF_3 and Cr_2O_3, respectively) and analyzed them using MX_6 cluster model with O_h symmetry. We took the polarization dependence (i.e. the polarized and depolarized configurations) into account both in the experiment and calculation, and the results were compared with a previous one for the $3d^0$ system (TiO_2).

Using the schematic total energy level diagram, we explained the charge transfer effect in RXES of all $3d^n$ ($n = 0$, 1, 2 and 3) compounds. The elastic peak in RXES corresponds to the bonding state and the inelastic peaks to the nonbonding and antibonding states. The behavior of RXES, however, is different in each material, because the influence of the crystal field and multiplet coupling effect

change with the $3d$ electron number. In TiF_3, for example, the spectrum corresponding to the crystal field excitation is clearly seen as a single peak, which is absent in TiO_2, and the spectra, which are modified by the multiplet coupling effect, are also seen in VF_3 and Cr_2O_3.

The polarization dependence in RXES was investigated by group theoretical consideration. In the $3d^0$ and $3d^3$ systems, the transition to the ground state is allowed in the polarized configuration, but forbidden in the depolarized one, whereas in the $3d^1$ and $3d^2$ systems, it is allowed both in the polarized and depolarized configurations. This means that in the $3d^0$ and $3d^3$ systems, the elastic peak appears only for the polarized configuration, but in the $3d^1$ and $3d^2$ systems the elastic peak appears both in the polarized and depolarized configurations. This is consistent with the numerical calculations and experimental results.

A drastic resonance enhancement corresponding to the excitation to the antibonding state in the $3d^0$ system is almost absent in the $3d^n$ ($n = 1$, 2 and 3) systems. This is due to the following two reasons. Firstly, the spectral intensity of the antibonding state depends on the hybridization strength, because weak hybridization suppresses the intensity of the antibonding state. In our parameter values, the hybridization effect in TiO_2 is much larger than that in TiF_3, VF_3 and Cr_2O_3. Secondly, the multiplet coupling effect in the intermediate state is also important, because the strong XAS satellite intensity induces the strong excitation to the antibonding state. If there are more than two electrons in the intermediate state, which corresponds to the $3d^n$ ($n = 1$, 2 and 3) systems, this effect broadens the whole structure of XAS spectrum and weakens the resonance enhancement. These two reasons were justified by numerical calculations for Cr_2O_3, where the parameter values were changed artificially and the multiplet coupling effect in the intermediate state was neglected.

Acknowledgment

This work is partially supported by a Grant-in-Aid for Scientific Research from the Ministry of Education, Culture, Sports, Science and Technology. One of authors (M.M.) is financially supported by JSPS Research Fellowships for Young Scientists.

1) C.-C. Kao, W. A. L. Caliebe, J. B. Hastings and J.-M. Gillet: Phys. Rev. B **54** (1996) 16361.
2) J. P. Hill, C.-C. Kao, W. A. L. Caliebe, M. Matsubara, A. Kotani, J. L. Peng and R. L. Greene: Phys. Rev. Lett. **80** (1998) 4967.
3) J. Jiménez-Mier, J. van Ek, D. L. Ederer, T. A. Callcott, J. J. Jia, J. Carlisle, L. Terminello, A. Asfaw and R. C. Perera: Phys. Rev. B **59** (1999) 2649.
4) S. Tanaka, K. Okada and A. Kotani: J. Phys. Soc. Jpn. **60** (1991) 3893.
5) A. Kotani and S. Shin: Rev. Mod. Phys. **73** (2001) 203.
6) P. Kuiper, J.-H. Guo, C. Såthe, L.-C. Duda, J. Nordgren, J. J. M. Pothuizen, F. M. F. de Groot and G. A. Sawatzky: Phys. Rev. Lett. **80** (1998) 5204.
7) Y. Harada, T. Kinugasa, R. Eguchi, M. Matsubara, A. Kotani, M. Watanabe, A. Yagishita and S. Shin: Phys. Rev. B **61** (2000) 12854.
8) M. Matsubara, T. Uozumi, A. Kotani, Y. Harada and S. Shin: J. Phys. Soc. Jpn. **69** (2000) 1558.
9) M. Watanabe, A. Toyoshima, Y. Azuma, T. Hayaishi, Y. Yan and A. Yagishita: Proc. SPIE **3150** (1997) 58.
10) Y. Harada, H. Ishii, M. Fujisawa, Y. Tezuka, S. Shin, M. Watanabe, Y. Kitajima and A. Yagishita: J. Synchrotron Radiat. **5** (1998) 1013.
11) M. Matsubara, T. Uozumi, A. Kotani, Y. Harada and S. Shin: in preparation.
12) T. Uozumi, K. Okada, A. Kotani, R. Zimmermann, P. Steiner, S. Hüfner, Y. Tezuka and S. Shin: J. Electron Spectrosc. Relat. Phenom. **83** (1997) 9.
13) M. Taguchi: Dr. thesis, Faculty of Science, The University of Tokyo, Hongo, Tokyo, 1997 [in Japanese].
14) O. Gunnarsson and O. Jepsen: Phys. Rev. B **38** (1988) 3568.
15) K. Okada and A. Kotani: J. Electron Spectrosc. Relat. Phenom. **71** (1995) R1.
16) T. Idé and A. Kotani: J. Phys. Soc. Jpn. **67** (1998) 3621.
17) S. Sugano, Y. Tanabe and H. Kamimura: *Multiplets of Transition-Metal Ions in Crystals* (Academic Press, New York, 1970) Chap. 6.